Detection of Radio-Frequency Interference for the Aquarius Radiometer

Sidharth Misra and Christopher S. Ruf, *Fellow, IEEE*

***Abstract*—A radio-frequency interference (RFI) detection algorithm has been developed for the Aquarius microwave radiometer. The algorithm compares individual brightness temperature samples with a local mean obtained from neighboring samples. If the sample under test significantly deviates from the local mean, then it is assumed to be corrupted by RFI. The algorithm has several adjustable parameters to optimize RFI detection. The performance of the algorithm has been characterized as a function of these parameters using a new form of RFI "ground truth" that is based on the kurtosis of the amplitude distribution of the predetected voltages of a radiometer. Ground-based radiometric data obtained from the JPL-PALS campaign were used to assess the performance of the algorithm. False-alarm rates and the dependence of false alarms on worst case naturally occurring brightness temperature variations on orbit are determined as functions of the adjustable parameters of the algorithm.**

***Index Terms*—Interference suppression, microwave radiometry.**

I. Introduction

THE AQUARIUS low Earth orbiting mission is intended to produce global maps of sea surface salinity (SSS) for use in climate studies. It includes a microwave radiometer operating at 1.4 GHz to measure SSS [2]. The contamination of radiometer data is possible if man-made sources of radio-frequency interference (RFI) are mistakenly detected and interpreted as natural thermal emission by the ocean surface. The presence of RFI has been noted in a number of spaceborne microwave radiometers at higher frequencies than that of Aquarius [4] and on airborne radiometers operating at the same frequency as Aquarius [1], [11]. The sensitivity of the observed L-band brightness temperature (TB) to climatically relevant changes in SSS is low enough that even quite small biases in the observations due to RFI can be detrimental to the mission objectives [8]. For this reason, the radiometer's data sampling rate has been increased by several orders of magnitude above the Nyquist rate suggested by the antenna-footprint size and the spacecraft orbital velocity [12]. This will significantly enhance the flexibility and sensitivity of an RFI "glitch detection" algorithm that will be included as part of the ground processing.

Manuscript received October 1, 2007; revised February 6, 2008. Current version published October 1, 2008. This work was supported in part by the National Aeronautics and Space Administration under Research Grants NNG04HZ28C and NNG05GL97G.

S. Misra is with the Department of Atmospheric, Oceanic and Space Sciences, University of Michigan, Ann Arbor, MI 48109 USA (e-mail: samisra@umich.edu).

C. S. Ruf is with the Department of Atmospheric, Oceanic and Space Sciences and the Space Physics Research Laboratory, University of Michigan, Ann Arbor, MI 48109 USA.

Digital Object Identifier 10.1109/TGRS.2008.920371

One previous RFI mitigation technique, which is known as "asynchronous pulse blanking," that takes advantage of high resolution in the temporal domain to detect and remove glitches in real time prior to detection, has been developed [10]. This algorithm has been adapted for use by the Aquarius mission. The Aquarius RFI detection algorithm operates on samples of the antenna temperature, after detection, at their raw (highest) sample rate. It is designed to detect individual samples that significantly differ from the local average value of those nearest neighbor samples that are themselves not corrupted by RFI. There are a number of parameters in the detection algorithm that can be adjusted to control its behavior. Those parameters affect the following: 1) the extent of the region surrounding a sample that constitutes its local neighborhood; 2) the magnitude of the difference between a sample and its local average, which indicates the presence of RFI; and 3) the "guard band" surrounding a sample with RFI that will also be flagged as potentially contaminated. In addition, optimal values for the parameters may vary depending on the proximity of a sample to a major coastline. The behavior of the detection algorithm can be characterized in several ways. The probability of false alarm characterizes excessive sensitivity, in which case RFI is indicated when it is not present. This possibility is more likely near a major coastline, when the natural variations in TB are greatest, than it is in the open ocean. The probability of missed detection characterizes the inadequate sensitivity of the algorithm to the presence of RFI. The settings of the parameters in the algorithm must weigh these two competing characteristics against one another in order to reach an acceptable compromise.

A series of field campaigns has recently been conducted with a new type of microwave radiometer that uses an agile digital detector (ADD) to measure both the second and fourth moments of the predetection voltage [3], [5], [6]. The second moment is the conventional measurement made by a square-law detector. The additional fourth-moment measurement allows the kurtosis of the voltage to be calculated. The kurtosis has been found to be a very reliable indicator of the presence of RFI, even when its power level is extremely low. Data from the ADD field campaigns, if taken at the proper sample rate, can be used as an experimental test bed for assessing the behavior of the Aquarius RFI detection algorithm as a function of its adjustable parameters. In particular, the availability of the kurtosis measurements allows for the experimental verification of the probability of false alarm of the algorithm, which is a statistic that is otherwise difficult to validate with confidence.

II. RFI Detection Algorithm

The algorithm works on the detection principle of flagging any sample above a certain threshold as being contaminated by

RFI. There are five steps involved in calculating the threshold and flagging a particular sample. The algorithm consists of four separate parameters that can be varied to control the detection performance.

Denoting x_i as the radiometric antenna temperature of the sample under test, a set of neighboring antenna temperature samples surrounding x_i is chosen to estimate its local mean value. The interval of time within which these samples lie is kept constant to keep the ground track distance covered by the antenna footprint constant. The number of Earth viewing samples taken during this time interval varies due to noise diode and ambient reference calibration samples that are interleaved between multiple Earth viewing samples. The number of neighboring samples to be used is determined by the parameter W_S (window-size). The set of neighboring antenna temperature samples associated with x_i is given by the following:

$$Y_i = \left[x_{\left(i-\frac{W_s}{2}\right)}, \ldots, x_{(i-1)}, x_{(i+1)}, \ldots, x_{\left(i+\frac{W_s}{2}\right)}\right] \quad (1)$$

where $i = [(W_s/2+1), \ldots, (N - W_s/2)]$ is the index of samples within the window W_S surrounding x_i. In order to keep the window symmetric about both sides of x_i, the parameter W_S is always an even integer. The set Y_i might have certain samples that have been flagged with RFI from previous tests. While calculating the local mean value of Y_i, such samples are not used. The local mean value of Y_i is defined as follows:

$$\widetilde{y}_i = \frac{\sum\limits_{j=\pm1,\pm2,\ldots,\pm\frac{W_s}{2}} x_{i+j} f_{i+j}}{\sum\limits_{j=\pm1,\pm2,\ldots,\pm\frac{W_s}{2}} f_{i+j}} \quad (2)$$

where $f_k = 0$ if antenna temperature sample x_k has been previously flagged as having RFI present and $f_k = 1$ if not. The local mean value calculated in this way is termed "dirty" because there might still be RFI-contaminated samples in Y_i that were not flagged. In order to obtain a local "clean" mean, a threshold filter is applied. The threshold is determined by using the local mean value given by (2) and a multiple of the radiometric uncertainty (noise equivalent delta temperature, NEΔT) of a single sample of the antenna temperature. For Aquarius, the NEΔT will vary with each of its three radiometers. The elements of Y_i are tested for RFI contamination and flagged if they exceed the threshold test given by the following:

$$f'_{i+j} = \begin{cases} 0, & \text{if } x_{i+j} \geq \widetilde{y}_i + T_m\sigma \\ 1, & \text{if } x_{i+j} \leq \widetilde{y}_i + T_m\sigma \end{cases} \quad (3)$$

where f'_k is the RFI flag for x_k, $j = [-W_s/2, \ldots, -1, 1, \ldots, W_s/2]$, σ is the NEΔT radiometric uncertainty of an individual sample of the antenna temperature, and the threshold level above which RFI is assumed to be present is $T_m\sigma$, where T_m (mean-threshold magnitude) is a scaling factor (not necessarily an integer). T_m is a variable parameter of the RFI algorithm. The remaining RFI-free elements of Y_i are averaged together to estimate the local clean mean value of x_i. This test removes any apparent RFI spikes present in Y_i, along with the naturally occurring tail end of the normally distributed signal. The local clean mean value is given by the following:

$$\widetilde{y}_{ci} = \frac{\sum\limits_{j=\pm1,\pm2,\ldots,\pm\frac{W_s}{2}} x_{i+j} f_{i+j} f'_{i+j}}{\sum\limits_{j=\pm1,\pm2,\ldots,\pm\frac{W_s}{2}} f_{i+j} f'_{i+j}}. \quad (4)$$

The sample under test x_i is then compared to the local clean mean using a second threshold test. If x_i deviates from the local clean mean by more than a certain multiple of the NEΔT, then it is considered to be contaminated by RFI and flagged accordingly. This test is given by the following:

$$f_i = \begin{cases} 0, & \text{if } x_i \geq \widetilde{y}_{ci} + T_{\det}\sigma \\ 1, & \text{if } x_i \leq \widetilde{y}_{ci} + T_{\det}\sigma \end{cases} \quad (5)$$

where the threshold level above which RFI is assumed to be present is given by $T_{\det}\sigma$, where $T_{\det}$ (detection-threshold magnitude) is a scaling factor (not necessarily an integer). $T_{\det}$ is also a variable parameter of the RFI algorithm. This detection threshold test is less strict than the previous mean threshold test (i.e., $T_{\det} > T_m$) because it directly results in discarded data, whereas the previous test only lowers the number of samples used to determine the local mean.

If x_i is flagged due to RFI, then a certain number of samples before and after x_i are also considered to be contaminated by RFI. This is to remove any RFI-contaminated samples in the near vicinity of a flagged sample that might be just below the detection threshold. The range of samples to be so flagged is determined based on the characteristic time scale with which signals can enter and leave the radiometer antenna beam versus the time interval between raw samples. This RFI flag can be expressed as follows:

$$f_{i+m} = 0, \qquad m = [-W_r, \ldots, -1, 1, \ldots, W_r] \quad (6)$$

where W_r (range window) is the range of samples so flagged. W_r is a fourth variable parameter of the detection algorithm.

III. Ground Truth and FAR

A ground-based campaign was conducted during April–May 2006 at the NASA Jet Propulsion Laboratory (JPL) to assess the performance of the ADD kurtosis detector for RFI detection and mitigation. Measurements were made using a hybrid radiometer consisting of the JPL-PALS RF front end [7] and University of Michigan ADD back end [5]. The sampling characteristics of the measurements and the controlled variation of the observed TB scene were similar to the expected conditions with Aquarius on orbit. The Aquarius data system will sample every 10 ms, which is similar to the PALS-ADD system. The spacecraft has a ground track velocity of 7.5 km/s, and the antenna-footprint dimensions of the three radiometer antenna patterns in the along-track direction are 85, 102, and 125 km. For the central 102-km footprint, it will, therefore, take approximately 13 s for the Aquarius TB to fully transition from ocean to land during a coastal crossing. During this time, roughly 1300 TB samples will be taken. This is mimicked in the data taken by PALS-ADD by sweeping a blackbody absorber over its antenna in 13 s. Due to these similarities, the

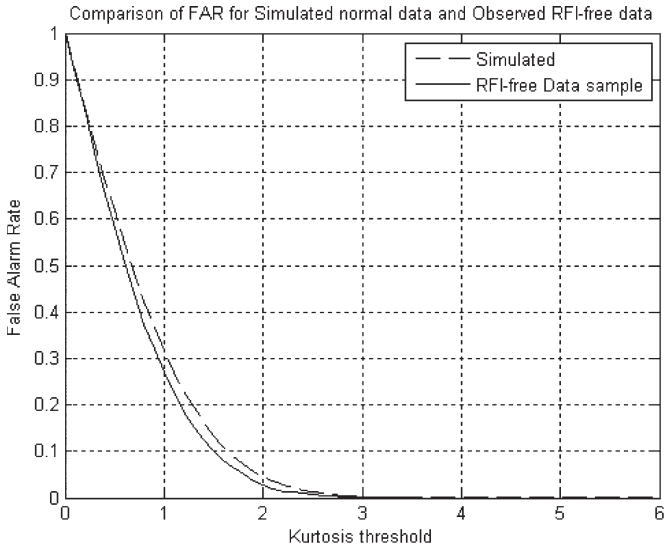

Fig. 1. FAR of the kurtosis detection algorithm for various thresholds calculated from (dashed line) normally distributed simulated data and (solid line) RFI-free PALS-ADD data sample.

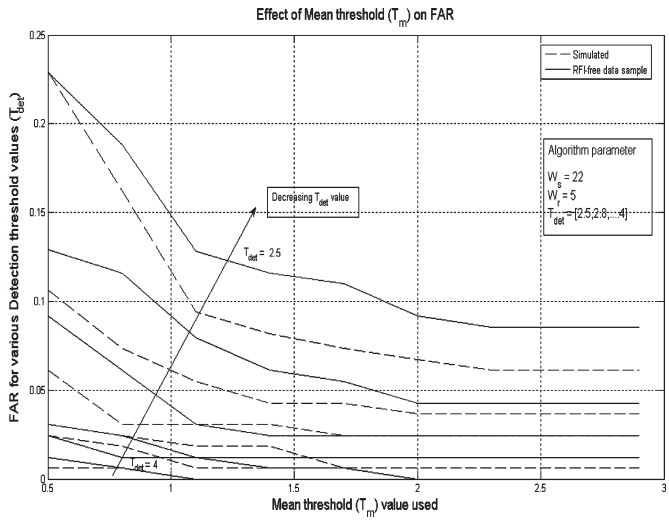

Fig. 2. Effects of mean-threshold magnitude T_m on the FAR of the second-moment detection algorithm for the detection-threshold magnitude $T_{\rm det}$ values (from lower left to upper right): $T_{\rm det} = 4.0$, 3.7, 3.4, 3.1, 2.8, and 2.5.

measurements can be used as a proxy for Aquarius flight data to assess the expected performance of the Aquarius RFI detection algorithm.

ADD measures the first four moments of the amplitude distribution of the predetected signal. The kurtosis parameter derived from these four moments is a reliable indicator for the presence or absence of RFI at or above NEΔT levels [5]. RFI detection by kurtosis serves as RFI ground truth for the assessment of the performance of the Aquarius RFI detection algorithm.

The performance of the algorithm with respect to its various adjustable parameters is assessed in terms of the false-alarm rate (FAR), which is the probability that RFI will be detected when it is not present. The FAR of the detection algorithm, which uses only the second moment, is obtained by comparing its results to the results obtained by using the kurtosis. It should be noted that the kurtosis algorithm itself has a FAR associated with it. The threshold for RFI detection by the kurtosis was chosen so as to produce an extremely low FAR. The kurtosis FAR is given by the following [9]:

$$\text{FAR} = 1 - \text{erf}\left(\frac{z}{\sqrt{2}}\right) \tag{7}$$

where erf() is the error function and z is the normalized kurtosis threshold in units of the theoretical standard deviation of the samples of kurtosis. In (7), it is assumed that the RFI thresholds above and below the mean are equidistant about it. The kurtosis FAR with respect to z is shown in Fig. 1. The dashed line is obtained by using simulated normally distributed data, and the solid line indicates values obtained by using an RFI-free portion of the PALS-ADD data. The curve based on observations is slightly lower than that predicted by (7) as a result of known quantization effects in the measurements [9].

For use as a ground truth reference, the kurtosis threshold is set at 3.7 times the standard error in the estimate of kurtosis (i.e., $z = 3.7$), which gives the kurtosis algorithm an extremely low FAR of 0.02% from (7). It should be noted that a lower FAR is accompanied by a lower probability of detection. As a result, even though the kurtosis algorithm is nearly error free, it cannot detect all RFI present.

Applying the second-moment detection and kurtosis algorithms to PALS-ADD measurements, it is observed that T_m and $T_{\rm det}$ have the greatest effect on FAR. Fig. 2 shows the FAR with a varying T_m value using normally distributed simulated data and RFI-free PALS data. The curves have been generated for different $T_{\rm det}$ while W_r and W_S are held constant. The result shown in Fig. 2 is intuitive. If we decrease T_m, high-amplitude second-moment data are discarded. The local clean mean is, hence, lower, which sets a lower second detection threshold, resulting in more data being flagged and higher FAR.

Similarly, $T_{\rm det}$ has a significant effect on the detectability of the second-moment detection algorithm. A sample is flagged as being contaminated by RFI whenever the second moment is above the threshold indicated by (5). The dependence of the FAR of the Aquarius detection algorithm on $T_{\rm det}$ is shown in Fig. 3. The FAR is obtained for different levels of T_m while W_r and W_S are held constant. As expected, a lower $T_{\rm det}$ makes the detection algorithm stricter, and as a result, more data are flagged and the FAR is increased. Because the second-moment data have a Chi-squared distribution, the proper detection threshold can be theoretically determined to produce a desired FAR.

W_S does not have a significant effect on the FAR of the detection algorithm. In a window that is densely populated with RFI, a larger window size would be helpful in detecting the local clean mean, whereas, in a sparsely RFI-populated data set, the sample window would have less of an effect.

IV. Performance of the Algorithm

PALS-ADD data were used as a proxy for Aquarius on-orbit data in order to characterize the performance to the Aquarius detection algorithm before launch. Fig. 4 is an example of data measured while viewing the nadir sky. The top panel indicates the second moment of the predetection signal. The estimated

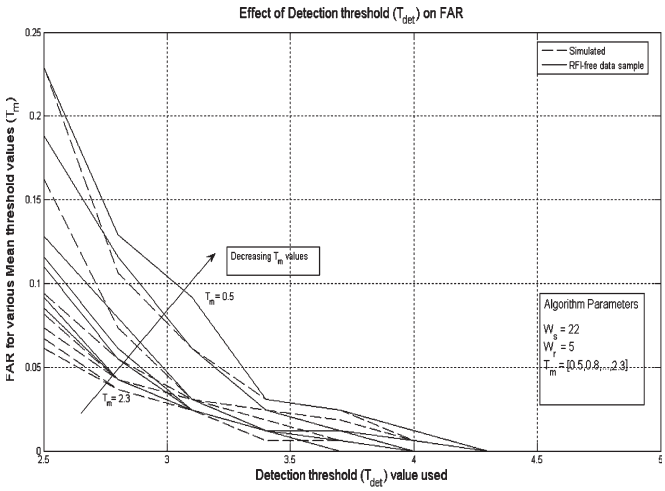

Fig. 3. Effects of detection-threshold magnitude $T_{\rm det}$ on the FAR of the second-moment detection algorithm for the mean-threshold magnitude T_m values (from upper right to lower left): $T_m = 0.5$, 0.8, 1.1, 1.4, 1.7, 2.0, and 2.3.

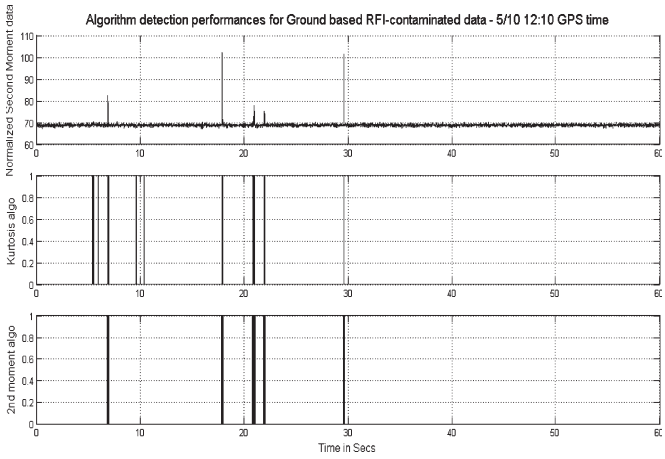

Fig. 4. RFI detection of PALS-ADD L-band radiometer measurements of nadir sky view with strong RFI present: (Top) Second-moment time series. (Center) Kurtosis of signal. (Bottom) Aquarius RFI detection algorithm.

value of second-moment data is proportional to the radiometer system noise temperature and includes contributions from the down-welling sky TB, thermal emission by the radiometer's antenna and the cabling between the antenna and receiver, and the noise temperature of the receiver itself. The second moment measured by ADD is equivalent to the Level 0 data product measured by conventional radiometers. The algorithm parameters used in the Aquarius detection algorithm for the following data sets are the following: $W_S = 20$, $T_m = 1.5$, $T_{\rm det} = 4$, and $W_r = 5$. These are candidate values for which the algorithm has a reasonably low FAR but is still able to detect most low level RFI. Other values that also yield satisfactory results are possible, and the determination of optimum values to be used will be an important task during the early phase of the on-orbit evaluation process for Aquarius. In the Aquarius flight processing implementation of the algorithm, all of the parameter values are adjustable as functions of longitude and latitude. This will permit them to be adjusted depending on the prevalence of RFI and the spatial variability of the TB (e.g., near a coastline or islands versus in open ocean).

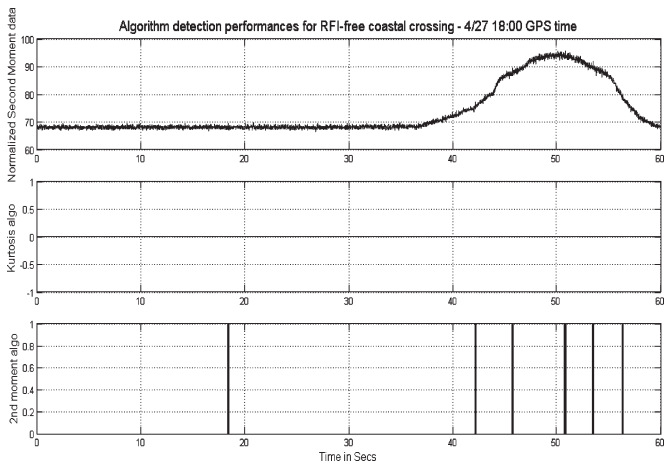

Fig. 5. RFI detection of PALS-ADD L-band radiometer measurements during transition from nadir sky view to blackbody absorber. (Top) Second-moment time series. (Center) Kurtosis of signal. (Bottom) Aquarius RFI detection algorithm.

There are clear spikes in the top panel of Fig. 4, which indicate the presence of RFI during daytime weekday operation at JPL. These RFI spikes are considered representative of the interference received by Aquarius because the radiometer integration time has approximately been matched with the pulsewidth of terrestrial radars operating within the relevant frequency range [12]. The kurtosis measurements are indicated by the center panel. A vertical bar is present whenever the algorithm detects an RFI-contaminated sample. The bottom panel indicates the results obtained from the second-moment detection algorithm. It can be observed that the clear RFI spikes that are visible in the second-moment data are detected by the Aquarius detection algorithm. The kurtosis algorithm flags a few other RFI-contaminated samples in the center panel that are near the NEΔT level. Such low-level RFI is missed by the second-moment detection algorithm.

It is informative to consider the performance of the Aquarius detection algorithm in terms of RFI false alarms during natural rapid TB changes such as a coastal crossing. A second PALS-ADD example is shown in Fig. 5, in which a blackbody absorber was slowly swept in front of the PALS antenna while looking at the nadir sky. The sweep rate approximates the rate at which the Aquarius footprint on orbit would cross over a coastline.

In the figure, the coastal crossing occurs at approximately the 45-s mark. The center panel shows that no RFI was present during this period. The bottom panel indicates a number of RFI false alarms, particularly in the vicinity of the most rapid changes in TB. This suggests that the algorithm's detection threshold may need to be varied geographically to make the detectability less sensitive when approaching rapid $d{\rm TB}/dt$ variations near coastlines.

The next example, shown in Fig. 6, starts with the same data set as in Fig. 5 and artificially introduces an RFI sample where the $d{\rm TB}/dt$ is highest (at approximately the 44-s mark). This is done to examine the performance of the algorithm in case an RFI source is located on the coastline. From Fig. 6, it can be seen that the second-moment detection algorithm successfully identifies the RFI-corrupted sample along with the other false alarms that were also present in Fig. 5. This verifies the ability

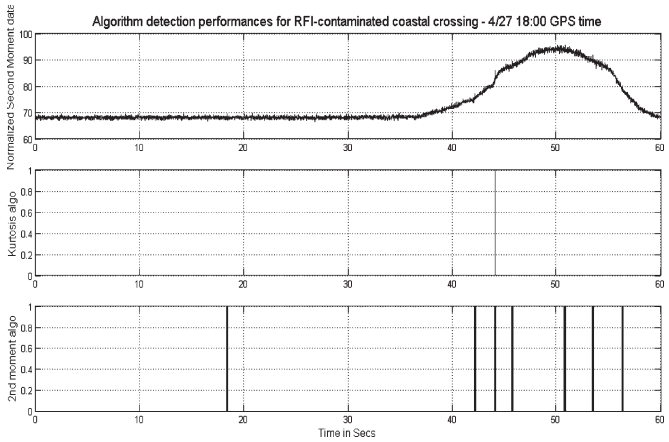

Fig. 6. Similar to Fig. 5 but with a single RFI event artificially added at the point of maximum time rate of change of TB during simulated coastal crossing. (Top) Second-moment time series. (Center) Kurtosis of signal. (Bottom) Aquarius RFI detection algorithm.

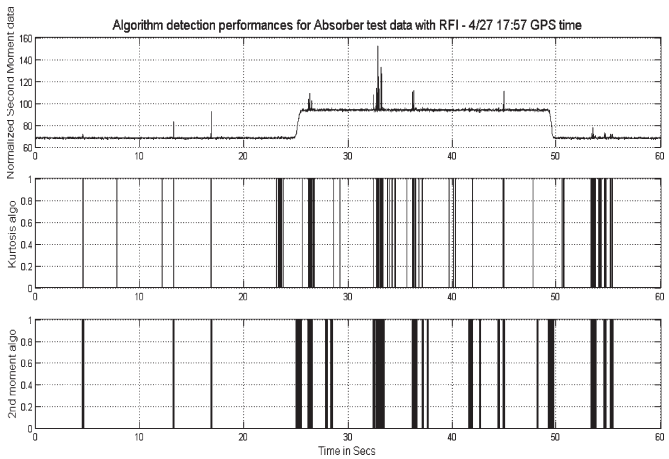

Fig. 7. RFI detection of PALS-ADD L-band radiometer measurements of nadir sky with blackbody absorber placed in front of the antenna for a while. (Top) Second-moment time series. (Center) Kurtosis of signal. (Bottom) Aquarius RFI detection algorithm.

of the detection algorithm to detect RFI with a rapidly changing background TB.

The performance of the Aquarius detection algorithm in the presence of both rapid TB changes and high levels of RFI was assessed by using the PALS-ADD data set shown in Fig. 7. During this particular minute of data, an absorber was temporarily placed in front of the PALS radiometer antenna and then removed. This results in a very high value of $d\mathrm{TB}/dt$, as seen in the top panel of the figure near the 25- and 49-s marks. The data were taken during the regular workday at JPL, during which time significant interference is often experienced. The RFI likely entered around the edges of the absorber, which was not tightly joined to the antenna, and into the radiometer. The kurtosis algorithm can be seen to pick up much more RFI than the second-moment detection algorithm in instances when the RFI perturbations are not easily distinguishable from the NEΔT fluctuations of the radiometer. Near the points of abrupt change in the second-moment data, the kurtosis data correctly do not flag the samples as being corrupted by RFI. On the other hand, the second-moment detection algorithm erroneously flags these samples as RFI. It should be noted that such rapid variations in TB, as are produced here, would not be produced in the case of Aquarius on orbit, taking into account its antenna beamwidth and ground track velocity.

V. Conclusion and Discussion

A second-moment detection algorithm is proposed that detects the presence of RFI-contaminated samples in the TB data of the Aquarius radiometer. The form of the algorithm could, with some modification, also be applied to other spaceborne radiometers for the removal of RFI. The algorithm works best if raw samples of the TB are made at a substantially greater rate than the Nyquist criteria set by the motion of the antenna footprint on the ground. This permits short duration radar interference to be better isolated and detected. For just this reason, a highly oversampled data rate is planned, for example, in the case of the L-band radiometer on the upcoming Soil Moisture Active Passive (SMAP) mission. SMAP is also considering incorporating a digital kurtosis detector into its design for added RFI detection capability. On the other hand, the L-band inteferometric radiometer on the upcoming Soil Moisture Ocean Salinity mission does not significantly oversample its data and, hence, would not be able to incorporate as effective a version of the second-moment detection algorithm [13].

The algorithm is a "glitch detector" in the sense that it compares a sample under test with a local mean obtained from neighboring samples and rejects the sample if it deviates too much from the local mean. The algorithm has four adjustable parameters that control the sensitivity of the detection. The first parameter is W_S, which defines the averaging window within which the local mean is computed. The mean threshold T_m then selects uncorrupted TB samples for calculating the local mean. The third parameter T_{det} sets the threshold with which the sample under test is compared and RFI is flagged. The last parameter W_r determines a range in the neighborhood of a contaminated sample within which samples are flagged with RFI even if they themselves do not set off the RFI flag.

Algorithm performance has been characterized by measuring the false-alarm rate while varying the algorithm parameters. The kurtosis of the radiometric predetection signal measured by using ADD has been used as a ground truth for flagging RFI. The kurtosis measurement can reliably identify the presence of RFI near the NEΔT radiometric noise floor. The performance of the Aquarius detection algorithm is assessed by comparing its results with the results obtained by using kurtosis detection. T_{det} and T_m parameters influence the FAR of the detection algorithm the most. RFI detection sensitivity can be increased with a lower T_{det}. In the absence of RFI, this will result in an increase in the FAR and in the number of data samples mistakenly flagged with RFI. With fewer data samples available, the NEΔT will be increased and radiometric sensitivity will be reduced. Thus, the proper setting of parameters such as T_{det} and T_m must balance between radiometric sensitivity and RFI detection sensitivity. It should be noted that false-alarm detections will, on average, produce a downward bias in TB because higher values are preferentially discarded. The resulting bias will increase with decreasing T_{det}.

Due to similarity with the Aquarius on-orbit sampling data, PALS-ADD ground data were taken as case-study examples

to assess the detection algorithm performance. The Aquarius detection algorithm can easily pick up high-level RFI spikes but is less effective when dealing with RFI at or near the NEΔT level of the radiometer for individual 10-ms samples. In most cases that are expected to be encountered on-orbit, this limitation will not have a significant impact on its ability to estimate SSS. The nominal integration time on which salinity measurements are based is approximately 6 s, i.e., approximately 600 of the individual 10-ms samples are averaged together. Therefore, the effects of the RFI corruption of a single 10-ms sample are reduced by a factor of 600 due to averaging. If a single 10-ms sample contains RFI at the NEΔT level, the corresponding error in the SSS estimate made from a 6-s sample is approximately 0.006 psu [8]. In comparison, the salinity retrieval uncertainty requirement for the Aquarius mission is 0.2 psu—more than one order of magnitude greater than the error due to RFI. It is possible, but unlikely, that many RFI-corrupted samples will be included in a 6-s integration period, due to the azimuthal sweep rate of typical ground scanning radars and the along-track motion of the Aquarius antenna footprint.

Regions near the coast are most likely to have terrestrial radars used for national defense and air-traffic safety. The performance of the detection algorithm in such areas is critical. The second moment has an enhanced susceptibility to erroneous detection of RFI (false alarms) when the TB of the scene under observation is changing rapidly, e.g., near a coastal crossing. In spite of a rapidly varying TB, the second-moment detection algorithm successfully detected the RFI that was present. This was tested by using a PALS-ADD data set that simulates the expected rate of change of TB when Aquarius would cross over a coastal region. The detection threshold can be adjusted to control the probability of false alarms and reduce sensitivity near coastal crossings, via the adjustable parameters T_m and T_{det}. It is anticipated that the Aquarius flight algorithm will have all these parameters dynamically adjusted as a function of the latitude and longitude of the antenna footprint to ensure better detectability.

ACKNOWLEDGMENT

The authors would like to thank the anonymous reviewers for their useful comments.

REFERENCES

[1] D. M. Le Vine, "ESTAR experience with RFI at L-band and implications for future passive microwave remote sensing from space," in *Proc. IGARSS*, Toronto, ON, Canada, 2002, pp. 847–849.

[2] D. M. Le Vine, G. S. E. Lagerloef, F. R. Colomb, S. H. Yueh, and F. A. Pellerano, "Aquarius: An instrument to monitor sea surface salinity from space," *IEEE Trans. Geosci. Remote Sens.*, vol. 45, no. 7, pp. 2040–2050, Jul. 2007.

[3] S. Misra, C. S. Ruf, and R. DeRoo, "Agile digital detector for RFI mitigation," in *Proc. Spec. Meeting Microw. Radiometry*, San Juan, Puerto Rico, Feb. 28–Mar. 3 2006, pp. 66–69.

[4] E. G. Njoku, P. Ashcroft, T. K. Chan, and L. Li, "Global survey and statistics of radio-frequency interference in AMSR-E land observations," *IEEE Trans. Geosci. Remote Sens.*, vol. 43, no. 5, pp. 938–947, May 2005.

[5] C. S. Ruf, S. M. Gross, and S. Misra, "RFI detection and mitigation for microwave radiometry with an agile digital detector," *IEEE Trans. Geosci. Remote Sens.*, vol. 44, no. 3, pp. 694–706, Mar. 2006.

[6] C. Ruf, S. Misra, S. Gross, and R. De Roo, "Detection of RFI by its amplitude probability distribution," in *Proc. IGARSS*, Denver, CO, Jul. 31–Aug. 4 2006, pp. 2289–2291.

[7] W. J. Wilson, S. H. Yueh, S. J. Dinardo, S. Chazanoff, F. Li, and Y. Rahmat-Samii, "Passive active L- and S-band (PALS) microwave sensor for ocean salinity and soil moisture measurements," *IEEE Trans. Geosci. Remote Sens.*, vol. 39, no. 5, pp. 1039–1048, May 2001.

[8] S. H. Yueh, R. West, W. J. Wilson, F. K. Li, E. G. Njoku, and Y. Rahmat-Samii, "Error sources and feasibility for microwave remote sensing of ocean surface salinity," *IEEE Trans. Geosci. Remote Sens.*, vol. 39, no. 5, pp. 1049–1060, May 2001.

[9] R. D. De Roo, S. Misra, and C. S. Ruf, "Sensitivity of the kurtosis statistic as a detector of pulsed sinusoidal RFI," *IEEE Trans. Geosci. Remote Sens.*, vol. 45, no. 7, pp. 1938–1946, Jul. 2007.

[10] N. Niamsuwan, J. T. Johnson, and S. W. Ellingson, "Examination of a simple pulse blanking technique for radio frequency interference mitigation," *Radio Sci.*, vol. 40, no. 5, p. RS5 S03, Jun. 2005.

[11] S. Misra, S. S. Kristensen, S. S. Søbjærg, and N. Skou, "CoSMOS: Performance of Kurtosis algorithm for radio frequency interference detection and mitigation," in *Proc. IGARSS*, Barcelona, Spain, Jul. 23–27, 2007, pp. 2714–2717.

[12] J. R. Piepmeier and F. A. Pellerano, "Mitigation of terrestrial radar interference in L-band spaceborne microwave radiometers," in *Proc. IGARSS*, Denver, CO, Jul. 31–Aug. 4 2006, pp. 2292–2296.

[13] Y. H. Kerr, P. Waldteufel, J.-P. Wigneron, J. Martinuzzi, J. Font, and M. Berger, "Soil moisture retrieval from space: The soil-moisture and ocean-salinity (SMOS) mission," *IEEE Trans. Geosci. Remote Sens.*, vol. 39, no. 8, pp. 1729–1735, Aug. 2001.

Sidharth Misra received the B.E. degree in electronics and communication engineering from the Nirma Institute of Technology, Gujarat University, Ahmedabad, Gujarat, India, in 2004 and the M.S. degree in electrical engineering and computer science—signal processing from the University of Michigan, Ann Arbor, in 2006. He is currently working toward the Ph.D. degree in the Department of Atmospheric, Oceanic and Space Sciences, University of Michigan.

He was a Research Engineer with the Space Physics Research Laboratory, University of Michigan, where he worked on the analysis and implementation of the agile digital receiver for RFI mitigation. He was also on Oceansat-II with the Space Applications Center, Indian Space Research Organization, Ahmedabad. He was a Research Assistant with the Danish National Space Center, Technical University of Denmark (DTU), Lyngby, performing RFI analysis for CoSMOS, which is an airborne campaign preparing for SMOS at DTU. His research interests involve signal detection and estimation, filter design, and image processing.

Christopher S. Ruf (S'85–M'87–SM'92–F'01) received the B.A. degree in physics from Reed College, Portland, OR, and the Ph.D. degree in electrical and computer engineering from the University of Massachusetts, Amherst.

He is currently a Professor of Atmospheric, Oceanic, and Space Sciences, a Professor of Electrical Engineering and Computer Science and the Director of the Space Physics Research Laboratory, University of Michigan, Ann Arbor. He was with Intel Corporation, Hughes Space and Communication, the NASA Jet Propulsion Laboratory, and Penn State University. In 2000, he was a Guest Professor at the Technical University of Denmark, Lyngby. He has published in the areas of microwave radiometer satellite calibration, sensor and technology development, and geophysical retrieval algorithms.

Dr. Ruf is a member of the American Geophysical Union (AGU), the American Meteorological Society (AMS), and Commission F of the Union Radio Scientifique Internationale. He has served or is serving on the Editorial Boards of the IEEE GRS-S NEWSLETTER, the AGU *Radio Science*, the IEEE TRANSACTIONS ON GEOSCIENCE AND REMOTE SENSING, and the AMS *Journal of Atmospheric and Oceanic Technology*. He was the recipient of three NASA Certificates of Recognition and four NASA Group Achievement Awards as well as the 1997 GRS-S Transactions Prize Paper Award, the 1999 IEEE Judith A. Resnik Technical Field Award, and the IGARSS 2006 Symposium Prize Paper Award.